PORE PRESSURE AND FLUID DETECTION FROM COMPRESSIONAL- AND SHEAR-WAVE DATA

JACK DVORKIN

ABSTRACT

By analyzing experimental data we show that in many room-dry rocks, the Poisson's ratio (PR) decreases with decreasing differential pressure (confining minus pore pressure). In many liquid-saturated rocks the opposite is true: PR increases with decreasing differential pressure. This means that in gas-saturated rocks, PR decreases with increasing pore pressure and in liquid-saturated rocks it increases with increasing effective pressure. We confirm the generality of the observed effect by theoretically reproducing it via effective medium modeling. This effect can be used as a new tool for seismic pore pressure and pore fluid monitoring during production as well as for overpressure detection from surface seismic, cross-well, sonic logs and measurements ahead of the drill bit.

INTRODUCTION AND PROBLEM FORMULATION

Typically, elastic-wave velocity in dry rock is measured in the laboratory by varying confining pressure while maintaining constant pore pressure. Because velocity reacts to the differential (confining minus pore) pressure (e.g., Wyllie et al., 1958), such data can be used to predict in-situ velocity variations in rock with gas due to pore pressure changes at constant overburden (Figure 1). Velocity at in-situ saturation conditions can be calculated from the dry-rock velocity using fluid substitution equations (e.g., Gassmann, 1951). Due to the large compressibility of gas, the in-situ velocity in rock with gas is very close to that in rock with air in the laboratory at the same differential pressure. Laboratory velocity-versus-pressure data combined with fluid substitution can be used to predict rock elastic property changes in reservoirs during production, which result from pore pressure and pore fluid temporal and spatial variations (Figure 2). Also, these data are a basis for interpreting seismic measurements for pore pressure and fluid variation in time and space (e.g., Wang et al., 1998; Tura and Lumley, 1999).

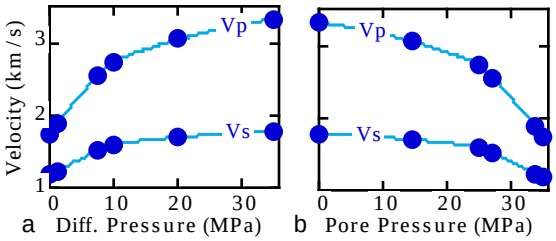

Figure 1. (a) Velocity versus differential pressure in ultrasonic laboratory experiments on a room-dry clay-free sandstone sample of 18% porosity. (b) Same data re-plotted versus (fictitious) pore pressure assuming that the overburden is 35 MPa and differential pressure changes due to changing pore pressure.

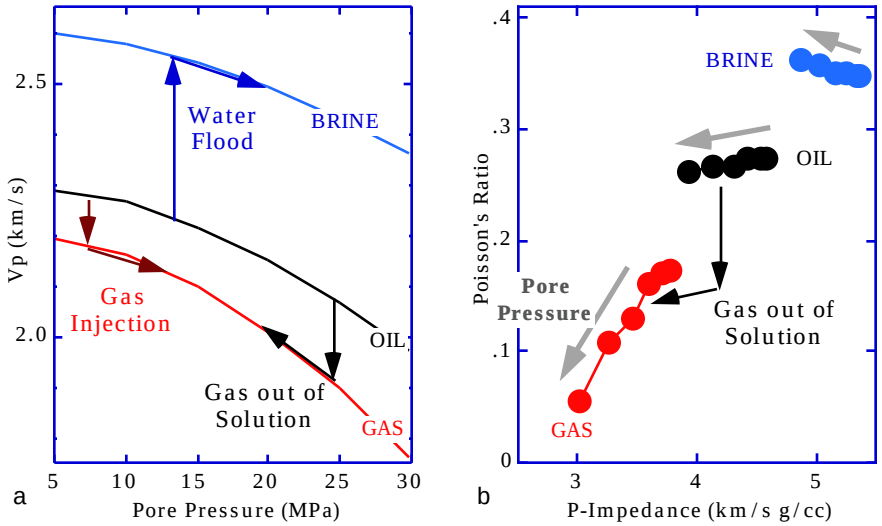

Figure 2. Laboratory velocity data for a sand sample from the North Sea Troll field (Blangy, 1992). (a) Velocity versus pore pressure assuming that the confining pressure is 30 MPa. The curves are produced by applying Gassmann's fluid substitution equation to the dry-rock data. Arrows show velocity variation during three different production scenarios. For example, during gas injection, oil is replaced by gas and pore pressure increases; during water flood, oil is replaced by water and pore pressure increases; during gas-out-of-solution drive, oil is replaced by gas and pore pressure decreases. The graph has to be treated as a scheme because it does not account for residual water, oil, and gas saturation. (b) Poisson's ratio versus P-wave impedance. Bold gray arrows show the direction of pore pressure increase. Only the gas-out-of-solution production scenario is shown.

The time scale of laboratory experiments, such as shown in Figure 1, is much smaller than the geologic time scale of overpressure development. Still, the laboratory experiments where pressure changes rapidly can be used to model the important transient (late-stage) overpressure mechanisms that are invoked when the pressure of the fluid in the rock mass is allowed to increase relative to hydrostatic through (a) aquathermal fluid expansion; (b) hydrocarbon source maturation and fluid expulsion; (c) clay diagenesis; (d) fluid pumping from deeper pressured intervals; and (e) decrease in overburden due to tectonic activity (Huffman, 1998).

The decrease in the P-wave velocity with increasing pore pressure has been used for overpressure detection (e.g., Grauls et al., 1995; Moos and Zwart, 1998). However, velocity does not uniquely indicate pore pressure because it also depends, among other factors, on porosity, mineralogy, and texture of rock. An example is given in Figure 3a where, at the same differential pressure of 20 MPa and in the same porosity range, velocity in gas-saturated Gulf sandstones is smaller than that in room-dry North Sea sands, due to textural differences. At the same time, velocity in the Gulf sandstones at 20 MPa is about the same as in the overpressured (5 MPa differential pressure) North-Sea sandstones (Figure 3b). The low velocity in the former sandstone group may be mistakenly attributed to overpressure.

We propose to resolve this ambiguity and improve the reliability of seismically detecting pore pressure changes during production as well as overpressure detection by using the Poisson's ratio (PR) calculated from the P- and S-wave velocity as a pore

pressure indicator. In the above example it uniquely reacts to pressure changes. In Figure 2c, the PRs of the two sandstone groups are in the same range at 20 MPa differential pressure, whereas their velocity ranges are different. At the same time, in Figure 2d where the data for one group are at 20 MPa and for the other at 5 MPa, their PR ranges are different, while their velocity ranges are the same. PR in the North Sea sandstones decreases with decreasing differential pressure (increasing pore pressure at constant overburden).

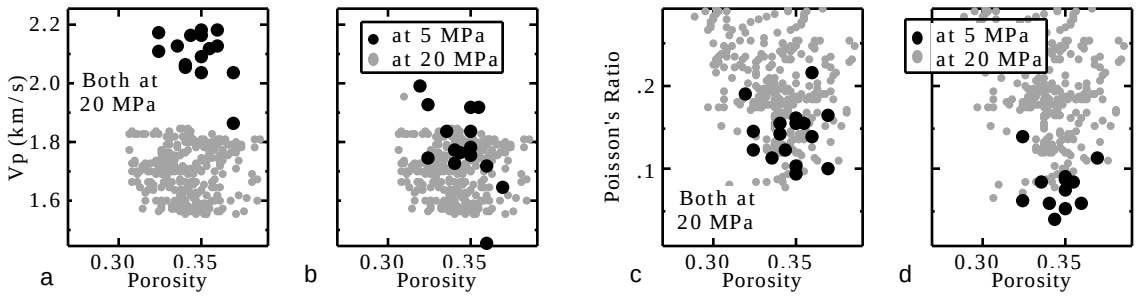

Figure 3. Compressional-wave velocity (a and b) and Poisson's ratio (c and d) versus porosity for North Sea sandstones (black circles) and Gulf sandstones with gas (gray symbols). The North Sea laboratory data are from Blangy (1992); the Gulf sandstone data are from a well log (discussed in Dvorkin et al., 1999) at about 20 MPa differential pressure. In a and c, North Sea data shown at 20 MPa (same as the Gulf data). In b and d, North Sea data shown at 5 MPa (the Gulf data are at 20 MPa).

Below, we show that this PR-pressure effect persists in many sandstones as well as in other rock types and suggest practical ways of using it for pore pressure monitoring and overpressure prediction.

POISSON'S RATIO AND PRESSURE IN ROCKS WITH GAS

PR (ν) can be calculated from the compressional- and shear-wave velocity (V_p and V_s, respectively) as

$$\nu = 0.5(V_p^2 / V_s^2 - 2) / (V_p^2 / V_s^2 - 1). \qquad (1)$$

Nur (1969) was probably first to record the decrease of PR with decreasing differential pressure in room-dry granite (Figure 4a) and dolomite samples. Toksoz et al. (1976) also present this effect and propose to use Poisson's ratio to identify saturating fluids. Nur and Wang (1989) state that the V_p / V_s ratio in gas-saturated rocks increases with increasing differential pressure. Wang (1997) supports this statement by laboratory velocity measurements in carbonate samples.

This effect appears to be general and can be observed in many sandstone and sand samples. Data from some of them are given in Figure 4 where the porosity range is between zero and 40% and the clay content range is between zero and 45%. The compressional-wave velocity varies significantly among these samples but PR invariably decreases with decreasing differential pressure. Data collected on about 50 sandstone samples are summarized in Figure 5a where the dry-rock PR at 30 MPa and 5 MPa differential pressure is plotted versus porosity. The ranges of the low-pressure and high-

pressure PR do not significantly overlap. At the same time, depending on porosity, mineralogy, and texture, the low-pressure velocity in some samples may be in the same range as the high-pressure velocity in others (Figure 5b). The PR-pressure effect is highlighted in Figure 5c where the 30 MPa data are plotted versus the 5 MPa data. The former are invariably larger than the latter.

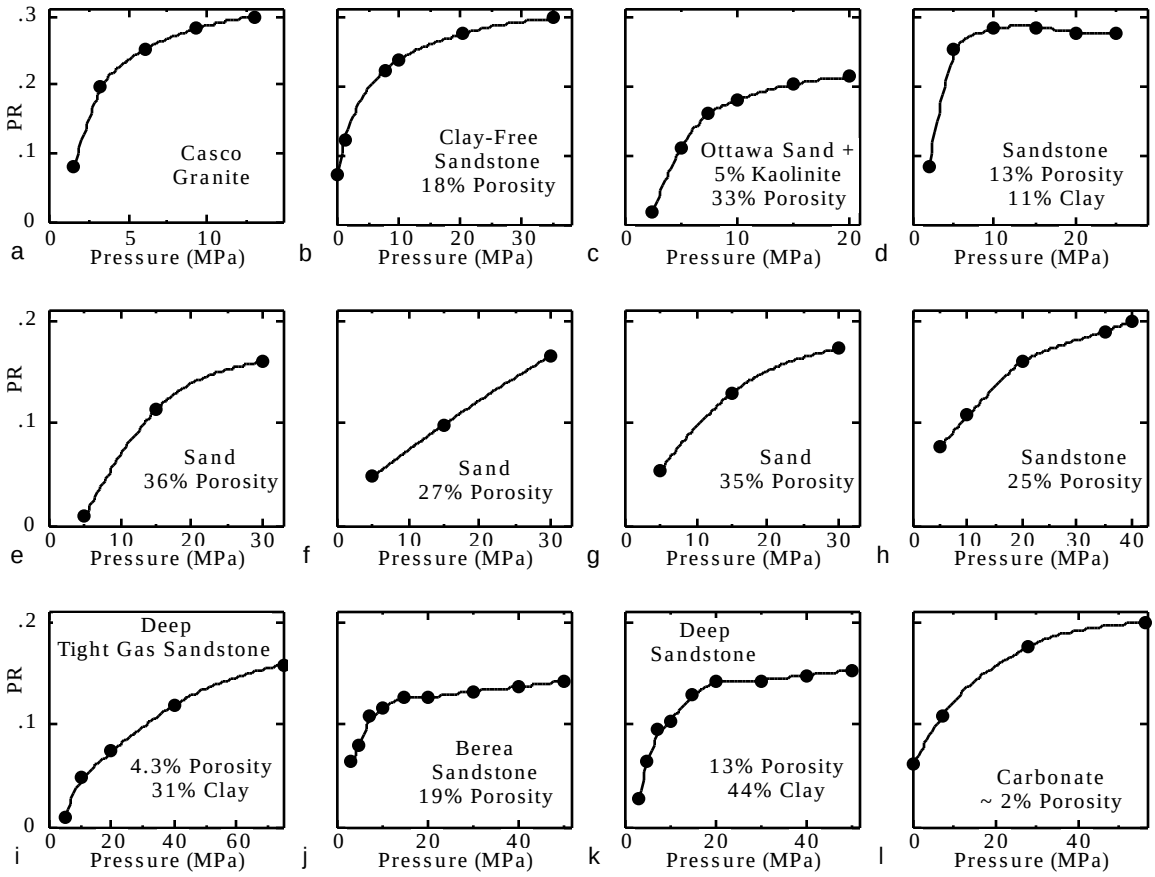

Figure 4. PR versus differential pressure in room-dry samples. Data used are from Nur (1969), Yin (1993), Han (1986), Blangy (1992), and authors' database.

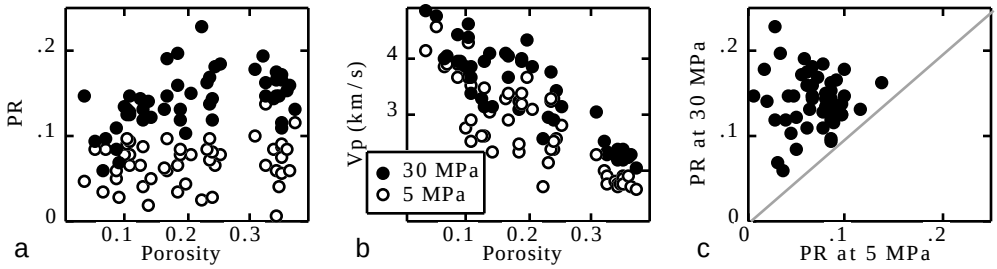

Figure 5. Data collected on about 50 room-dry sandstone samples. Sources same as in Figure 4. PR (a) and compressional-wave velocity (b) versus porosity. Filled symbols are for 30 MPa, open symbols are for 5 MPa. c. PR at 30 MPa versus PR at 5 MPa.

To theoretically explain the observed effect of PR decreasing with decreasing

differential pressure, we assume that the observed velocity and elastic moduli variations versus pressure are due to the closure (as differential pressure increases) and opening (as differential pressure decreases) of compliant thin cracks in the rock. We numerically simulate the effect of differential pressure on elastic moduli in a sandstone sample used in Figure 1. Specifically, we assume that the porosity occupied by thin cracks of 0.001 aspect ratio decreases from 1% at zero differential pressure to zero at 35 MPa. We introduce an elastic body whose bulk and shear moduli are the same as of the sample selected at 35 MPa, and then populate it with the cracks gradually increasing the crack porosity from zero to 1%. The effective medium theory we use to calculate the elastic moduli of the body with cracks is the self-consistent approximation (SC) of Berryman (1980).

The modeling results shown in Figure 6 not only qualitatively but also quantitatively mimic the laboratory data (as long as the pressure to crack porosity transform is correct). Our mathematical modeling is consistent with the observed effect of pressure on Poisson's ratio and establishes the generality of the phenomenon. This theoretical explanation of the effect under examination should be valid for many granular rocks where compliant grain contacts resemble thin cracks and compliant cracks may be present within the grains.

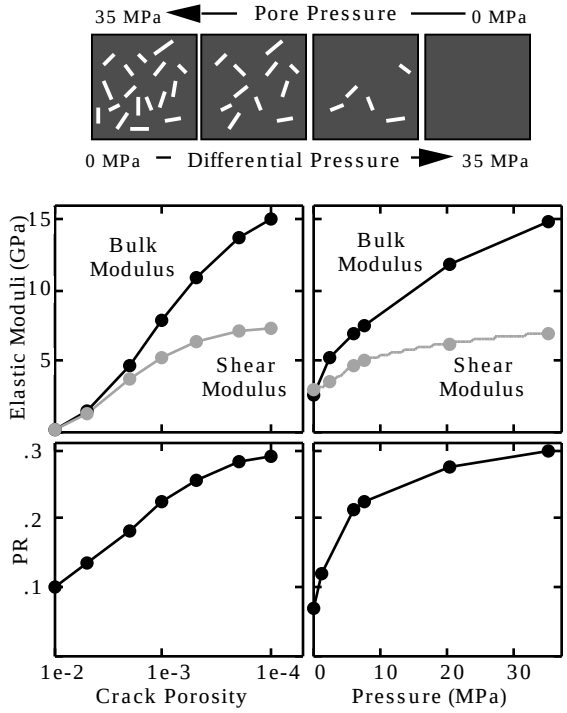

Figure 6. Theoretical modeling of pressure effect on the elastic moduli of the room-dry sandstone sample from Figure 1. Top cartoon: crack opening and closure as pressure changes. Left column: theoretical bulk and shear moduli (top) and PR (bottom) versus crack porosity. Right column: experimental bulk and shear moduli and PR versus differential pressure.

It is important to emphasize that the essence of the effective medium modeling of rock is the replacement of the actual rock that has a very complex microstructure with an

idealized body that retains the salient microstructural features and exhibits similar mechanical behavior. This is why we model the effect of pressure on PR by assuming that the rock under examination contains microcracks with a single aspect ratio. A similar mathematical effect can be achieved by assuming a different aspect ratio or a distribution thereof.

The simulated decrease of the dry-rock PR with increasing pore pressure has a physical basis (Pennington, 2000). Let us assume that the smaller the differential pressure the larger the number of compliant microcracks in the solid under examination. Let us also assume that the sample is isotropic and, therefore, the microcracks are isotropically oriented in space (Figure 7). As the sample is loaded in the axial direction, the microcracks partly accommodate this deformation and thus act to reduce the sample's sideways expansion as compared to the case where the microcracks are absent. The more microcracks are present the smaller the sideways deformation and the smaller the Poisson's ratio.

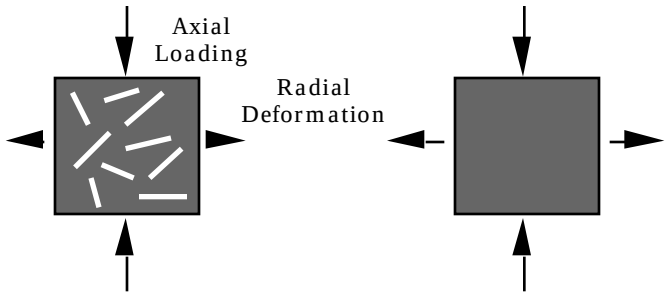

Figure 7. For the same axial deformation, the radial deformation in the sample with cracks (left) is smaller than in the sample without cracks (right). So is Poisson's ratio.

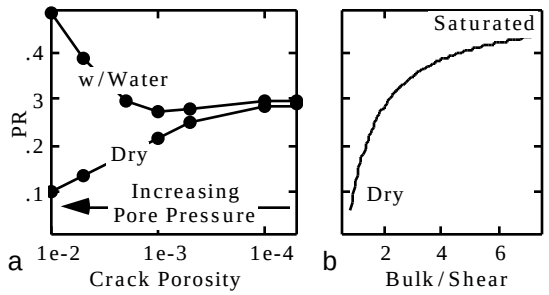

Figure 8. (a) Theoretical modeling of pressure effect on the dry-rock and rock-with-water PR in a synthetic calcite sample. PR versus crack porosity. Higher crack porosity corresponds to low differential or high pore pressure. (b) PR versus the bulk to shear modulus ratio. The low bulk to shear ratio is typical for dry rock whereas the high ratio is typical for soft fluid-saturated rock.

In our other (purely synthetic) example, we assume that the sample at high differential pressure is calcite of 15% porosity and the pores are spherical and filled with high-compressibility gas. Using SC, we find that the PR of this sample is 0.29. Next we assume that the sample's porosity at low differential pressure is 16% and the additional 1% is due to thin cracks of 0.001 aspect ratio. By varying the crack porosity from zero (at high pressure) to 1% (at low pressure), we model the effect of pressure on PR (Figure

8a). We use Gassmann's (1951) equations to calculate PR in the water-saturated calcite sample where the bulk modulus of the water is 2.5 GPa. Notice that while the dry-rock PR decreases with increasing crack porosity (increasing pore pressure), the saturated-rock PR shows the opposite trend (Figure 8a).

POISSON'S RATIO AND PRESSURE IN ROCKS WITH LIQUID

The simulated increase of the saturated-rock PR with increasing pore pressure (Figure 8) has a physical basis. The higher the pore pressure, the softer the rock and the larger the relative increase in the bulk modulus between dry and water-saturated samples. With the shear modulus being the same for the dry and saturated rock (Gassmann, 1951), PR is larger in the saturated than in the dry sample (Figure 8b), especially in soft rock. An example of the saturated-rock PR increasing with decreasing differential pressure is given in Figure 9a. However, one may observe the opposite effect as well (Figure 9b). The direction of the saturated-rock PR change depends on the porosity and elastic moduli of the sample and has to be tested by using fluid substitution with the dry-rock data.

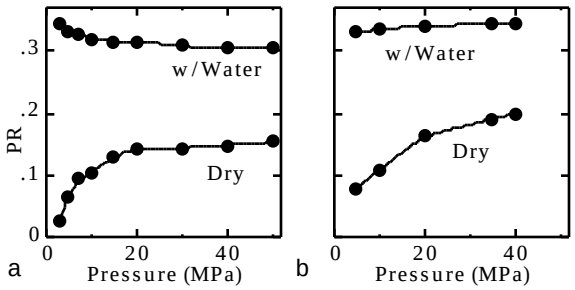

Figure 9. PR in dry and water-saturated samples versus differential pressure for (a) sample used in Figure 4k and (b) sample used in Figure 4h.

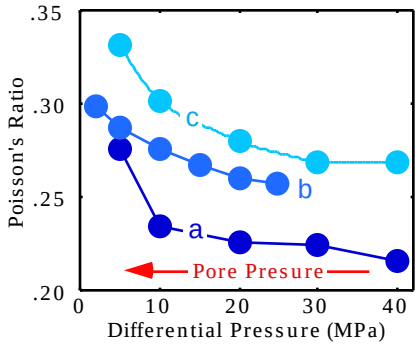

Figure 10. PR versus differential pressure in water-saturated shales. (a) sample of 24% porosity and 22% clay content; (b) shale from La Cira field in Colombia; (c) sample of 6% porosity and 24% clay content. Data in (a) and (c) are from ultrasonic measurements on water-saturated rocks (Han, 1986). Data in (b) are calculated from dry-rock measurements using Gassmann's (1951) fluid substitution equations.

Laboratory data for three water-saturated shale samples are summarized in Figure 10. In these rocks, Poisson's ratio increases with the decreasing differential and increasing

pore pressure. It is apparent that the ranges of Poisson's ratio variation are different in different samples. It is likely to be site-specific and depend on porosity, texture, and mineralogy.

DIAGNOSTIC CHARTS

Elastic rock properties (e.g., P-wave impedance and Poisson's ratio) can be obtained from seismic data using acoustic and elastic impedance inversion (e.g., Connolly, 1998). It is, therefore, important to create rock physics based charts that will help interpret these results in terms of pore pressure and pore fluid. An example of a diagnostic charts is given in Figure 11, based on laboratory measurements of the elastic-wave velocity in unconsolidated North Sea sands (Blangy, 1992). Different regions in the PR versus P-wave impedance plane and plane correspond to different pore pressure and pore fluid. One can identify both pore pressure and pore fluid from seismic (and separate the pore pressure effect from the pore fluid effect) by superimposing seismic elastic rock properties on a diagnostic chart. Note that diagnostic charts have to be site- and rock-type-specific.

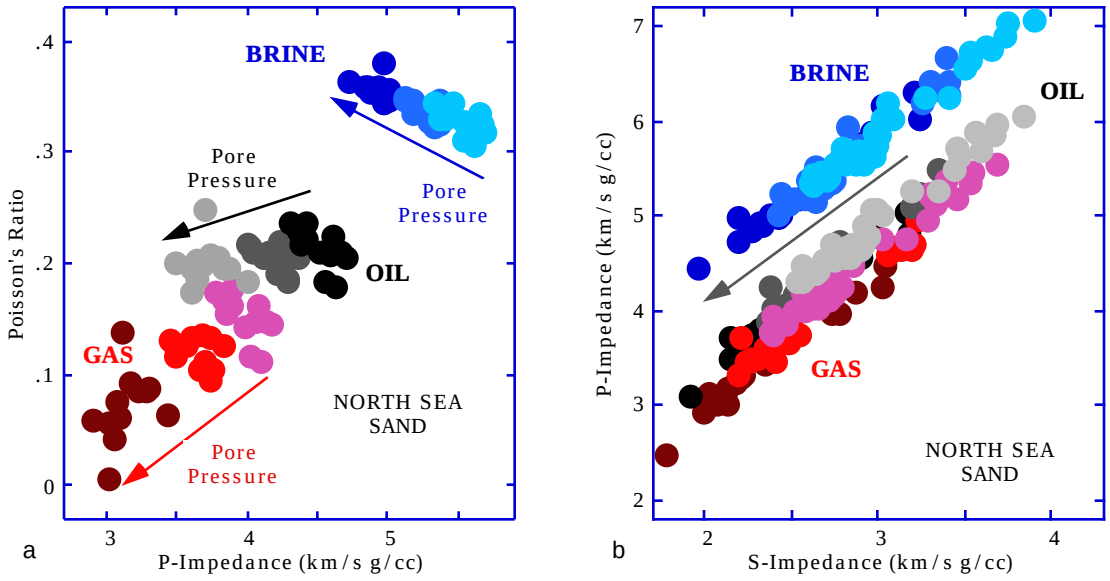

Figure 11. Pore pressure and pore fluid diagnostic charts. Based on dry-rock data and Gassmann's equations. (a) PR versus P-wave impedance for gas, oil, and brine and at varying differential pressure (5, 15, and 30 MPa). (b) Same data in a P-wave impedance versus S-wave impedance cross-plot. Arrows show the direction of pore pressure increase (differential pressure decrease).

ASSUMPTIONS AND CAVEATS

The pore pressure monitoring and overpressure detection technique proposed here is based on assumptions that are identical to those used in earlier overpressure prediction techniques. One is that the elastic-wave velocity in rock is a function of the differential pressure rather than the effective pressure (the latter term explained in, e.g., Rice and Cleary, 1976). This assumption is valid in many practical cases where the bulk modulus

of the rock's dry frame is much smaller than that of the solid phase.

Another assumption is that laboratory velocity measurements conducted under the hydrostatic state of stress can be used to predict velocity in situ where, in general, the state of stress is not hydrostatic. This assumption is commonly used in the industry because the non-hydrostatic-stress experiments are complicated and the actual in-situ stress tensor is, generally, unknown. This is why the hydrostatic confining pressure in the laboratory is taken as the analog of the in-situ lithostatic pressure (the overburden). Caution has to be exercised in applying the proposed method of pore pressure monitoring and overpressure prediction where the in-situ state of stress strongly deviates from the hydrostatic state.

EFFECT OF TEXTURE

In order to emphasize the importance of calibrating rock's pressure behavior to rock type, we compare the laboratory data for soft North Sea sands used in Figure 11 to those of stiff, slightly cemented, North Sea sands (Strandenes, 1991). The samples in both data sets have high porosity. However, the P-wave impedance in the slightly cemented samples is significantly larger than that in the soft samples (Figure 12). Dvorkin and Nur (1996) show that this elastic property difference is due to small amounts of quartz cement present at the grain contacts in the stiff sands.

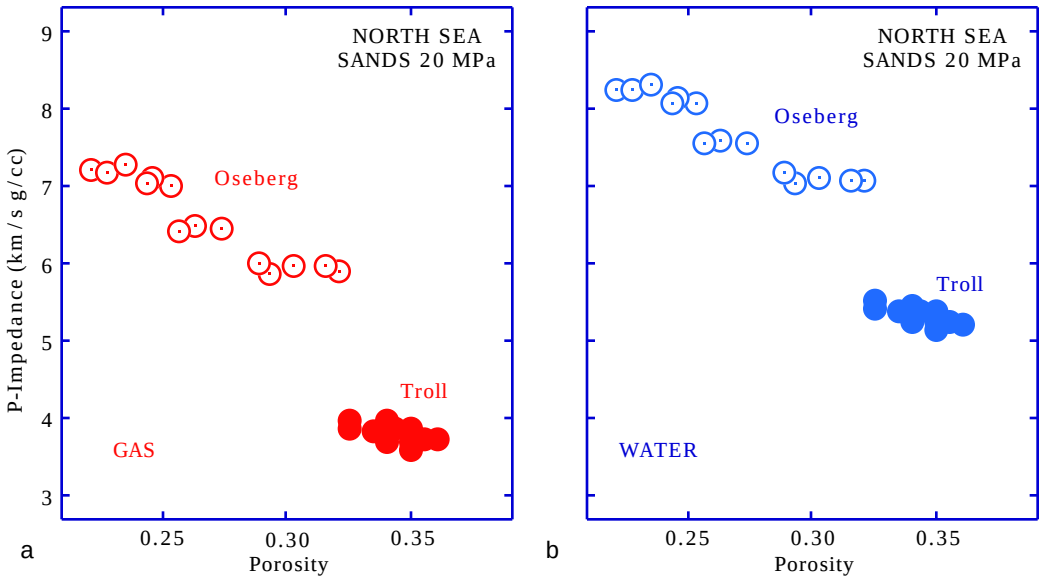

Figure 12. P-wave impedance versus porosity for soft Troll sands (filled symbols) and stiff Oseberg sands (open symbols). The data are at 20 MPa differential pressure. (a) Room-dry samples; (b) water-saturated values calculated from the room-dry sample data using Gassmann's (1951) equations. The Troll data are from Blangy (1992) and the Oseberg data are from Strandenes (1991).

Poisson's ratio is plotted versus the P-wave impedance for the two sand groups in Figure 13a at a constant (20 MPa) differential pressure. It is compared to the pressure behavior of the soft sand data set reproduced in Figure 13b (same as Figure 11a). The behavior of Poisson's ratio at a constant pressure, as the rock type changes from slightly

cemented (Oseberg) to completely unconsolidated (Troll) has the same character as the behavior that corresponds to pore pressure increase in completely unconsolidated (Troll) sands.

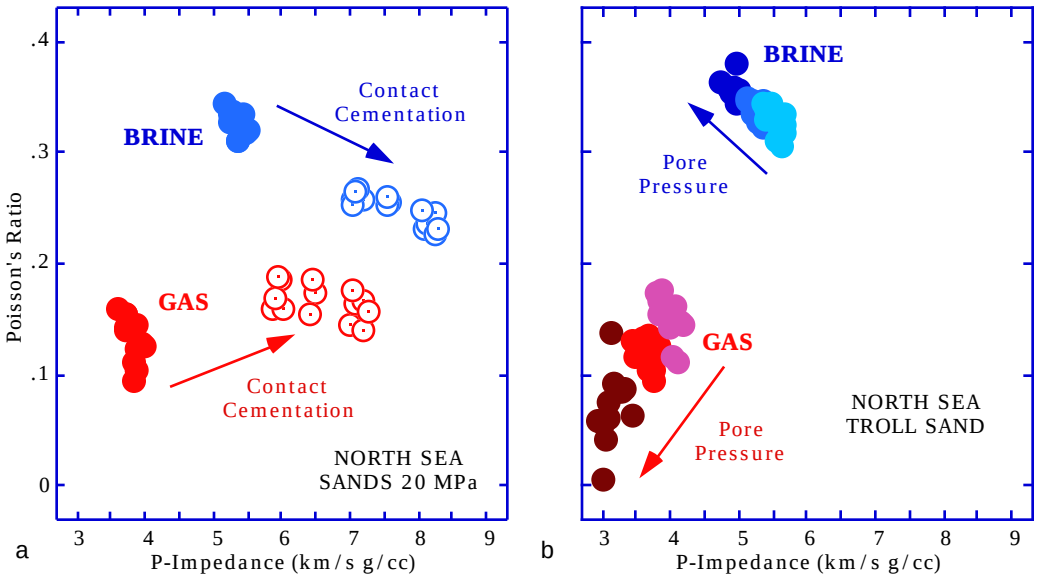

Figure 13. Poisson's ratio versus P-wave impedance in North Sea sands. (a) Differential pressure is constant (20 MPa). Filled symbols are for the Troll samples and open symbols are for the Oseberg samples. Red symbols are for the room-dry samples and blue symbols are for water-saturated samples. The effect of saturation is modeled using Gassmann's (1951) equations. (b) Same as Figure 11, without oil-saturated samples

CONCLUSION

The recent progress of geophysical measurement technology can allow one to extract shear-wave data from surface and marine (bottom cables) reflection profiling, well logs, and cross-well measurements, and, in the future, from measurements ahead of the drill bit. Because of this, the observed and theoretically confirmed effect of Poisson's ratio decreasing with increasing pore pressure in rocks with gas can be used as a physical basis for a new method of pore pressure and pore fluid monitoring and overpressure detection. This effect was probably implicitly used by Pigott et al. (1990) and Pigott and Tadepalli (1996) in estimating pressure from AVO inversion in carbonates and clastics.

The new method offered here can be used to improve the reliability of traditional methods and their recent modifications (e.g., Bowers, 1994; Moos and Zwart, 1998) where only the compressional-wave velocity and density or porosity are used and the shear-wave velocity is used to correct for fluid effects. The effect of pore pressure on the saturated-rock Poisson's ratio can be accurately calculated from the dry-rock data and then used for overpressure prediction as well. Laboratory measurements on representative site-specific rock samples should allow one to quantify and calibrate the observed effects. Everything said here about PR applies to the V_p / V_s ratio as well.

ACKNOWLEDGMENTS

We thank Dr. Wayne Pennington and Dr. Dan Moos for constructive comments.

REFERENCES

Berryman, J.G., Long-wavelength propagation in composite elastic media, I and II, J. Acoust. Soc. Amer., 68, 1809-1831, 1980.

Blangy, J.P., Integrated seismic lithologic interpretation: The petrophysical basis, Ph.D. thesis, Stanford University, 1992.

Bowers, G.L., Pore pressure estimation from velocity data: Accounting for overpressure mechanisms besides under-compaction, IADC/SPE 27488, 1994.

Connolly, P., 1998, Calibration and inversion of non-zero offset seismic, SEG 68th Annual Meeting, Expanded Abstracts, AVO 1.5, 182-184.

Dvorkin, J., and Nur, A., 1996, Elasticity of High-Porosity Sandstones: Theory for Two North Sea Datasets, Geophysics, 61, 1363-1370.

Dvorkin, J., Moos, D., Packwood, J., and Nur, A., 1999, Identifying patchy saturation from well logs, Geophysics, 64, 1756-1759.

Gassmann, F., Elasticity of porous media: Uber die elastizitat poroser medien, Vierteljahrsschrift der Naturforschenden Gesselschaft, 96, 1-23, 1951.

Grauls, D., Dunand, J.P., and Beaufort, D., Predicting abnormal pressure from 2-D seismic velocity modeling, Proceedings OTC Conference, Houston, 1995.

Han, D.-H., Effects of porosity and clay content on acoustic properties of sandstones and unconsolidated sediments, Ph.D. thesis, Stanford University, 1986.

Huffman, A.R., The future of pressure prediction using geophysical methods, in Pressure regimes in sedimentary basins and their prediction, Conference proceedings, Houston, 1998.

Moos, D., and Zwart, G., Predicting pore pressure from porosity and velocity, in Pressure regimes in sedimentary basins and their prediction, Conference proceedings, Houston, 1998.

Nur, A.M., Effect of stress and fluid inclusions on wave propagation in rock, Ph.D. Thesis, MIT, 1969.

Nur, A., and Wang, Z., Seismic and acoustic velocities in reservoir rocks. Volume 1, Experimental studies, SEG Geophysics reprint series 10, 1989.

Pennington, W., 2000, Personal communication.

Pigott, J.D., Shrestha, R.K, and Warwick, R.A., Direct determination of carbonate reservoir porosity and pressure from AVO inversion, SEG 60th Annual Int. Meeting, Extended Abstracts, 2, 1533-1536, 1990.

Pigott, J.D., and Tadepalli, S.V., Direct determination of clastic reservoir porosity and pressure from AVO inversion, SEG 66th Annual Int. Meeting, Extended Abstracts, 2, 1759-1762, 1996.

Rice, J.R., and Cleary, M.P., Some basic stress diffusion solutions for fluid-saturated elastic porous media with compressible constituents, Rev. Geophysics and Space Physics, 14, 227-241, 1976.

Strandenes, S., Rock physics analysis of the Brent Group Reservoir in the Oseberg Field, Stanford Rock Physics and Borehole Geophysics Project, 1991.

Toksoz, M.N., Cheng, C.H., and Timur, A., Velocities of seismic waves in porous rocks, Geophysics, 41, 621-645, 1976.

Tura, A., and Lumley, D.E., 1999, Estimating pressure and saturation changes from time-lapse AVO data, SEG 69th Annual Meeting, Expanded Abstracts, SRC 4.2.

Wang, Z., Seismic properties of carbonate rocks, in Carbonate Seismology, Palaz, I., and

Marfurt, K., eds., SEG Geophysical developments series, 6, 29-52, 1997.
Wang, Z., Cates, M.E., and Langan, R.T., 1998, Seismic monitoring of a CO2 flood in a carbonate reservoir: A rock physics study, Geophysics, 63, 1604-1617.
Wyllie, M.R.J., Gregory, A.R., and Gardner, G.H.F., An experimental investigation of factors affecting elastic wave velocities in porous media, Geophysics, 23, 459-493, 1958.
Yin, H., Acoustic velocity and attenuation of rocks: isotropy, intrinsic anisotropy, and stress induced anisotropy, Ph.D. thesis, Stanford University, 1993.